# THE STUDY OF GaN MATERIALS FOR DEVICE APPLICATIONS

by

YAM FONG KWONG

Thesis submitted in fulfilment of the
requirements for the degree
of Doctor of Philosophy

January, 2007

## ACKNOWLEDGEMENTS

First and foremost, I would like to express my sincere gratitude to my main supervisor, Dr Zainuriah Hassan, for her valuable guidance and dedicated support throughout the course of this project. She is not only my supervisor but mentor and advisor in this research work. As the project progresses, many unexpected technical difficulties surface, especially some events of the research programme do not go as planned, however, she tried exhaustively to create conducive research environments by providing all the necessary resources, and this led to the successful completion of this project eventually. Apart from that, I am very thankful to her for appointing me as a research officer; with this appointment, my financial burden is greatly eased. I also would like to thank my co-supervisor, Dr Azlan Abdul Aziz for his kind assistance in this project.

Much of this work would have been virtually impossible without the technical support from our helpful laboratory assistants. I would like to take this opportunity to thank Ms Ee Bee Choo and Mr Mohtar Sabdin

Particularly important in this research project is my group of fellow-buddies, Lee Yan Cheung, Nor Zaini, Tan Chee Kiat, Lim Cheong Wan, Surina Othman, Khairul Azwan, Oh Sue Ann, and Ooi Hean Team. They have contributed many ideas in my research work. We have also shared a lot of wonderful moments in the campus and eventually this journey of study in USM becomes unforgettable in my life. Also not to be forgotten are Ng Sha Shiong and Sin Yew Keong, their sincere assistances in many areas have helped me a lot in sample preparation, experimental set up and technical paper writing

Finally, I would like to thank my dearest wife, Paun Cher Yin, for her encouragement, patience and understanding. Without her support, I will not be able to complete my study.

# TABLE OF CONTENTS


| | Page |
|---|---|
| **ACKNOWLEDGEMENTS** | ii |
| **TABLE OF CONTENTS** | iii |
| **LIST OF TABLES** | ix |
| **LIST OF FIGURES** | xi |
| **LIST OF SYMBOLS** | xv |
| **LIST OF MAJOR ABBREVIATION** | xvii |
| **ABSTRAK** | xix |
| **ABSTRACT** | xxi |
| **CHAPTER 1 : INTRODUCTION** | **1** |
| 1.1 Introduction to III-nitrides | 1 |
| 1.2 Historical Development of Nitrides | 2 |
| 1.3 Research Background | 4 |
| 1.4 Research Objectives | 6 |
| 1.4.1 Originality of the research works | 7 |
| 1.5 Outline of the Thesis | 8 |
| **CHAPTER 2 : LITERATURE REVIEW** | **9** |
| 2.1 Introduction | 9 |
| 2.2 Nitride Epitaxial Growth Techniques | 9 |
| 2.2.1 Hydride Vapor Phase Epitaxy (HVPE) | 9 |
| 2.2.2 Metalorganic Chemical Vapour Deposition (MOCVD) | 10 |
| 2.2.2.1 Atmospheric pressure MOCVD | 11 |
| 2.2.2.2 Low pressure MOCVD (LPMOCVD) | 12 |
| 2.2.2.3 Plasma-anhanced MOCVD (PA-MOCVD) | 13 |
| 2.2.3 Molecular Beam Epitaxy (MBE) | 14 |
| 2.2.3.1 MBE growth kinetics | 15 |
| 2.2.3.2 The strengths of MBE | 16 |
| 2.3 Factors Influencing GaN Crystalline Quality | 17 |
| 2.3.1 Substrates | 17 |
| 2.3.2 Buffer layer | 20 |

2.4 Overview of Metal-GaN contact technology 22
2.4.1 Ohmic contact on GaN 22
2.4.2 Schottky contact on GaN 23
2.5 The Development of Porous GaN 25

**CHAPTER 3: THEORY** **28**
3.1 Introduction 28
3.2 Principle of the Characterization Tools 28
3.2.1 Atomic force microscopy 29
3.2.2 Scanning electron microscopy and Energy dispersive x-ray spectroscopy 31
3.2.2.1 Scanning electron microscopy 31
3.2.2.2 Energy dispersive x-ray spectroscopy 33
3.2.3 X-ray diffraction 34
3.2.4 Hall Effect 35
3.2.5 Photoluminescence 36
3.2.6 UV-visible spectroscopy 37
3.2.7 Raman Spectroscopy 39
3.3 Principle of the Metal Coating and Plasma Etching Techniques 40
3.3.1 Thermal evaporation 40
3.3.2 Sputtering system 40
3.3.3 Reactive ion etching and inductively couple plasma etching 41
3.4 Theory of Metal-semiconductor Contact 42
3.4.1 Current flow mechanism 42
3.4.2 Ohmic contact and specific contact resisyivity 44
3.4.2.1 The derivation of specific contact resistivity 44
3.4.3 Schottky contact and barrier height 46
3.4.3.1 The derivation of Schottky barrier height 46
3.5 Porous Semiconductor Generation Mechanisms 48
3.5.1 Photo-assisted electrochemical etching 48
3.5.2 Metal-assisted electroless chemical etching 49
3.6 Principle of GaN-based Devices 49
3.6.1 Gas sensor 49
3.6.1.1 Hydrogen gas sensing mechanism 50
3.6.1.2 The determination of sensitivity 52
3.6.2 GaN-based photodetectors 52

3.6.2.1 Metal-semiconductor-metal (MSM) photodiode 52
3.6.2.2 Performance of the MSM photodetector 54
3.6.3 Light emitting diode 54

**CHAPTER 4: METHODOLOGY** **57**

4.1 Introduction 57
4.2 Method in Studying Material Properties 57
4.2.1 Growth conditions 57
4.2.1.1 GaN films grown by low-pressure MOCVD (LP-MOCVD) 57
4.2.1.2 GaN films grown by plasma-assisted MOCVD (PA-MOCVD) 58
4.2.1.3 Commercial GaN films 58
4.2.2 Characterization 58
4.3 Method in Studying Metal Contacts 59
4.3.1 Wafer Cleaning 59
4.3.2 Metallization 59
4.3.2.1 Thermal evaporation 59
4.3.2.2 D.C. sputtering 60
4.3.3 Different types of metal contact studies and characterization 61
4.4 Method in Studying Porous GaN 63
4.4.1 Porous GaN prepared by UV assisted electrochemical etching 63
4.4.1.1 Fabrication condition 64
4.4.2 Porous GaN prepared by Pt assisted electroless etching 64
4.4.2.1 Fabrication condition 65
4.4.3 Characterization 65
4.4.4 Study of the influence of porous GaN layer on Pt Schottky contacts 66
4.5 Fabrication and Characterization of Devices 66
4.5.1 Gas sensor 67
4.5.1.1 Fabrication of catalytic gas sensor 67
4.5.1.2 Experimental set up and characterization 67
4.5.2 MSM photodetector 68
4.5.2.1 Fabrication of MSM photodetector 68
4.5.2.2 Characterization 69

4.5.3 Light emitting Schottky diodes 69
4.5.3.1 Fabrication of light emitting Schottky diodes 69
4.5.3.2 Probing condition 70
4.5.3.3 Characterization 71
4.5.4 Light Emitting Diodes (LED) 71
4.5.4.1 Etching of GaN p-n homojunction light emitting structure 71
4.5.4.2 Characterization 72
4.6 Instrumentations 72
4.6.1 Scanning electron microscopy (SEM) 72
4.6.2 Atomic force microscopy (AFM) 72
4.6.3 High resolution x-ray diffraction (HR-XRD) 73
4.6.4 Photoluminescence (PL) and Raman 73
4.6.5 UV-Vis spectroscopy 74

**CHAPTER 5: RESULTS AND DISCUSSIONS : THE STUDY OF MATERIAL PROPERTIES 75**

5.1 Introduction 75
5.2 Study of GaN Films Grown by Low Pressure MOCVD 75
5.2.1 Scanning electron microscopy 75
5.2.2 X-ray diffraction 76
5.2.3 Photoluminescence 77
5.2.4 Raman scattering 78
5.3 Study of GaN Films Grown by Plasma Assisted MOCVD at Low Temperature with Addition of H-plasma 80
5.3.1 Scanning electron microscopy and atomic force microscopy 80
5.3.2 X-ray diffraction 82
5.3.3 Energy dispersive spectroscopy 83
5.3.4 Photoluminescence 84
5.3.5 Raman scattering 86
5.3.6 Hall effect measurement 87
5.4 Study of Commercial GaN Films 87
5.4.1 Structural measurements 88
5.4.2 Optical measurements 89
5.5 Summary 90

**CHAPTER 6: RESULTS AND DISCUSSIONS : THE STUDY OF METAL CONTACTS** **91**

6.1 Introduction 91
6.2 Study of Metal Contacts on n-GaN 91
6.2.1 Scanning electron microscopy 91
6.2.2 Energy dispersive x-ray spectroscopy 92
6.2.3 Current-voltage measurements 93
6.3 Study of Metal Contacts on p-type GaN 95
6.3.1 Ni/Ag ohmic contacts on p-GaN 95
6.3.1.1 Specific contact resistivities 95
6.3.2 Ti- and Ag-based Schottky contacts on p-GaN 98
6.3.2.1 Electrical characteristics 98
6.4 Summary 100

**CHAPTER 7: RESULTS AND DISCUSSIONS: THE STUDIES OF POROUS GaN PROPERTIES** **102**

7.1 Introduction 102
7.2 Porous GaN Properties Prepared by UV Assisted Electrochemical Etching 102
7.2.1 Scanning electron microscopy 102
7.2.2 Atomic force microscopy 104
7.2.3 High resolution XRD 105
7.2.4 Photoluminescence 107
7.2.5 Optical transmission 109
7.2.6 Raman scattering 111
7.3 Porous GaN Properties Prepared by Platinum Assisted Electroless-chemical Etching 113
7.3.1 Scanning electron microscopy 113
7.3.2 Atomic force microscopy 115
7.3.3 High resolution XRD 116
7.3.4 Photoluminescence 117
7.3.5 Optical transmission 118
7.3.6 Raman scattering 120
7.4 Influence of Porous Layer on Pt Schottky Contacts 122

7.4.1 Morphological, structural and electrical properties 123
7.5 Summary 128

**CHAPTER 8: RESULTS AND DISCUSSIONS: DEVICES** **132**

8.1 Introduction 132
8.2 Gas Sensor 132
8.2.1 Electrical and structural properties 133
8.3 MSM Photodetector 138
8.3.1 Electrical characteristics 139
8.4 Light Emitting Schottky Diodes Based on p-GaN 141
8.4.1 Electroluminescent characteristics 142
8.4.2 The origin of different light emissions 145
8.5 GaN p-n Homojunction Light Emitting Diodes 147
8.5.1 Electrical and morphological characteristics 147
8.6 Summary 149

**CHAPTER 9: CONCLUSION AND FURTHER STUDIES** **151**

9.1 Conclusion 151
9.2 Future Studies 152

**REFERENCES** **155**

**APPENDICES** **165**

Appendix 1: The fundamental properties of wurtzite III-nitride semiconductors at room temperature. 165

Appendix 2: Carrier Transport Mechanisms and Schottky Contact on Porous Semiconductor 166

Appendix 3: The derivation or determination of absorption coefficient, $\alpha$, energy band gap, $E_g$ and refractive index, $n$ from UV-Vis spectroscopy 168

Appendix 4: Schottky Barriers 172

**LIST OF PUBLICATIONS** 174

# LIST OF TABLES


| | | Page |
|---|---|---|
| Table 2.1: | Lattice parameters and thermal expansion coefficient of prospective substrates for nitrides epitaxial growth. (Data extracted from Popovici and Morkoc 2000) | 18 |
| Table 2.2: | Lattice mismatch between GaN and the most commonly used substrates. | 19 |
| Table 2.3: | The overview of some published data on metal contacts/p-GaN. | 23 |
| Table 3.1: | Electrical Nature of Ideal MS contacts. (adapted from Pierret, 1996) | 42 |
| Table 4.1: | Type of characterizations for GaN samples from different sources. | 58 |
| Table 4.2: | Scope of study, metal contacts, thermal treatment and characterization of n- and p-GaN samples. | 62 |
| Table 4.3: | Anodization conditions of the samples. | 64 |
| Table 4.4: | Porous GaN generated by two different techniques are investigated by various characterization tools. | 65 |
| Table 4.5 | Samples under different type of treatments are analyzed by various characterization tools. | 66 |
| Table 4.6: | Different probing conditions for various samples. | 70 |
| Table 5.1: | EDS data for SI-1 and SI-2. | 84 |
| Table 6.1: | EDS analysis data of oxygen for different samples under different annealing temperatures. | 93 |
| Table 6.2: | The specific contact resistivities at different annealing temperatures and times. | 96 |
| Table 7.1: | The surface roughness (root mean square) of the samples measured by AFM. | 105 |
| Table 7.2: | The diffraction peak positions of (0002) and $(10\bar{1}2)$ planes, lattice constants of different samples derived from XRD measurements. | 106 |
| Table 7.3: | The peak position, FWHM, peak shift and the relative intensity of near band edge PL of different samples. | 109 |
| Table 7.4: | Peaks position of $E_2$(high), $A_1$(TO) and $E_1$(TO) of different samples obtained from Raman spectra. | 112 |
| Table 7.5: | The surface roughness (root mean square) of the samples measured by AFM. | 116 |
| Table 7.6: | The diffraction peak positions of (0002) and $(10\bar{1}2)$ planes, lattice constants of different samples derived from XRD measurements. | 117 |
| Table 7.7: | The peak position, FWHM, peak shift and the relative intensity of near band edge PL of different samples. | 118 |
| Table 7.8: | Peaks position of $E_2$(high), $A_1$(TO) and $E_1$(TO) of different samples obtained from Raman spectra. | 122 |
| Table 7.9: | The surface roughness (root mean square) of the sample surface and Pt contact layer of different samples measured by AFM. | 125 |
| Table 7.10: | The x-ray diffraction peak position and FWHM of (0002) plane for different samples. | 126 |
| Table 7.11: | The SBH and current at 3V and -3V of different samples. | 127 |

| | | |
|---|---|---|
| Table 7.12: | Comparison of the structural and optical properties of porous GaN generated by two different techniques. | 130 |
| Table 8.1: | The Schottky barrier height of the porous GaN and as-grown GaN under different conditions. | 134 |
| Table 8.2: | The sensitivity of the two gas sensors operating at room temperature and 100°C under a constant voltage of 2V. | 136 |
| Table 8.3: | The ideality factor, SBH and dark and photo-current of as-grown and porous samples. | 140 |
| Table 8.4: | The probing condition, the emission color at different voltage and barrier height of various samples. | 144 |

# LIST OF FIGURES

| | | Page |
|---|---|---|
| Figure 1.1: | Number of publications (INSPEC) and activities in GaN over the years. (adapted from Akasaki, 2002). | 3 |
| Figure 2.1: | Schematic diagram of a vapor transport GaN growth reactor. (adapted from Pankove, 1973) | 10 |
| Figure 2.2: | The schematic diagram of a typical MOCVD growth reactor. (adapted from Akasaki and Amano 1997) | 10 |
| Figure 2.3: | The schematic diagram of the two-flow MOCVD reactor. (adapted from Nakamura *et al* 1991) | 12 |
| Figure 2.4: | The schematic diagram of the commercial vertical rotating disk LPMOCVD reactor. (adapted from Hassan and Kordesch, 2000) | 12 |
| Figure 2.5: | The schematic diagram of plasma-assisted MOCVD reactor. | 13 |
| Figure 2.6: | The schematic diagram of the MBE growth chamber. (Adapted from Franchi, *et al* 2003) | 14 |
| Figure 2.7: | Schematic illustration of the surface processes during growth in a MBE system. (Adapted from Herman and Sitter 1996) | 16 |
| Figure 2.8: | Reported barrier heights of metals to n-GaN as a function of their work function. (adapted from Liu and Lau, 1998) | 24 |
| Figure 3.1: | The setup of the fiber interferometer AFM system. (Adapted from Operating Manual, Surface Imaging System, 1999) | 29 |
| Figure 3.2: | Schematic of a typical SEM system. (adapted from Schroder, 1998) | 32 |
| Figure 3.3: | Elements in an EDX spectrum are identified based on the energy content of the x-rays emitted by their electrons as these electrons transfer from a higher-energy shell to a lower-energy one. (Adapted from manual of Thermo Scientific) | 33 |
| Figure 3.4: | Diffraction of x-rays by a crystal. (Adapted from William, 1994) | 34 |
| Figure 3.5: | The schematic diagram of an UV-visible spectrometer. (Adapted and re-drawn from the manual of Hitachi Double-Beam Spectrophotometer Model U-2000) | 38 |
| Figure 3.6: | Schematic description of (a) the thermionic emission, (b) thermionic field emission, and (c) tunneling mechanisms in an n-type semiconductor. $\phi_B$ is barrier height, and q is the charge of the electron. (Adapted from Morkoc, 1999) | 43 |

| | | |
|---|---|---|
| Figure 3.7: | (a)The transmission line pattern, and (b) the typical graph showing the variation of the resistance with respect to the gap distance. (Adapted from Morkoc, 1999) | 44 |
| Figure 3.8: | Schematic diagram of hydrogen adsorption process. (a) Formation of a polarization layer. (b) The corresponding schematic energy band diagram for the metal/GaN Schottky diode in air and upon exposing to hydrogen gases. (Adapted from Huang, *et al* 2005) | 50 |
| Figure 3.9: | Electron-hole pairs that have been generated at the gap between the two metal contacts (Schottky contacts) are then being separated by the electric field in the depletion region of the two Schottky contacts. (Adapted from Shur, 1996) | 53 |
| Figure 3.10: | p-n junction under (a) zero bias, and (b) forward bias. (Adapted from Schubert, 2003) | 56 |
| Figure 4.1: | The thermal evaporator. | 60 |
| Figure 4.2: | The D.C. sputtering system. | 61 |
| Figure 4.3: | The electrochemical etching experimental set up used to generate porous GaN. | 63 |
| Figure 4.4: | The electroless chemical etching experimental set up used to generate porous GaN. | 65 |
| Figure 4.5: | The schematic diagram of (a).Gas sensing system and (b) Gas chamber. | 67 |
| Figure 4.6: | The metal mask used to pattern the interdigitated Schottky contact for photodetector. | 68 |
| Figure 4.7: | (a) Top view, and (b) cross section view of ohmic and Schottky contacts of a typical Schottky diode sample. | 69 |
| Figure 5.1: | SEM micrographs: (a) SO1, and (b) SO2. Scale bar indicates 10 μm in length. | 75 |
| Figure 5.2: | XRD 2θ scan of (a) SO1 and (b) SO2. The insets show the enlargement of GaN (0002) reflection. | 76 |
| Figure 5.3: | Low temperature photoluminescence spectra of (a) SO1 and (b) SO2. | 78 |
| Figure 5.4: | Raman spectra of (a) SO1 and (b) SO2. | 79 |
| Figure 5.5: | SEM micrographs of GaN film (a) SI-1, (b) SI-2. Scale bar indicates 2 μm in length. | 80 |
| Figure 5.6: | AFM images of GaN film (a) SI-1 (b) SI-2. | 81 |
| Figure 5.7: | Phi scan of GaN film (a) SI-1, (b) SI-2. | 82 |

| | | |
|---|---|---|
| Figure 5.8: | The 2 theta-omega scan of GaN film (a) SI-1, (b) SI-2. | 82 |
| Figure 5.9: | The PL spectra of SI-1 and SI-2. | 85 |
| Figure 5.10: | The Raman spectra of SI-1 and SI-2. | 86 |
| Figure 5.11: | The SEM images of (a) n-GaN, and (b) p-GaN. | 88 |
| Figure 5.12: | The AFM measurements of (a) n-GaN, and (b) p-GaN. | 88 |
| Figure 5.13: | The XRD measurements of (a) n-GaN, and (b) p-GaN. | 89 |
| Figure 5.14: | The PL measurements of (a) n-GaN and, (b) p-GaN. | 89 |
| Figure 5.15: | The Raman spectra of (a) n-GaN and (b) p-GaN. | 89 |
| Figure 6.1: | SEM images of different samples annealed at 800°C for 15 minutes: (a) Co, (b) Ni, (c) Pt and (d) Ti. Scale bars indicate 5 $\mu$m. | 92 |
| Figure 6.2: | The I-V characteristics of different samples: (a) as-deposited, (b) annealed at 300°C, (c) annealed at 400°C; and (d) annealed at 500°C. | 94 |
| Figure 6.3: | SEM micrographs taken at different annealing temperatures under the same magnification, scale bar indicates 5 micron in length. | 97 |
| Figure 6.4: | The I-V characteristics of Schottky contacts on p-GaN (a) before heat treatment, and (b) after heat treatment. | 99 |
| Figure 7.1: | SEM images of different samples. (a) SN1, (b) SN2, (c) SN3, (d) SN4, (e) as grown and (f) low magnification of SN3. Same magnification for SEM images from (a) to (e). | 103 |
| Figure 7.2: | AFM micrographs of the porous GaN samples showing different surface topography. | 105 |
| Figure 7.3: | The near band edge PL spectra of different samples measured at room temperature. (a) As grown, (b) SN1, (c) SN2, (d) SN3 and (e) SN4. | 107 |
| Figure 7.4: | Optical transmission spectra of the samples (a) Full scale, (b) The enlargement. | 110 |
| Figure 7.5: | The Raman spectra of different samples: (a) Full spectra, and (b) zoom in area of 500 to 600 $cm^{-1}$. | 111 |
| Figure 7.6: | SEM images of the samples etched under different duration. (a) As grown, (b) 15 min, (c) 30 min, (d) 60 min, (e) 90 min, and (f) 90 min under high magnification. | 114 |
| Figure 7.7: | AFM micrographs of the porous GaN samples showing different surface topography. | 115 |

| | | |
|---|---|---|
| Figure 7.8: | The near band edge PL spectra of the samples etched under different durations measured at room temperature. | 117 |
| Figure 7.9: | Optical transmission spectra of the samples (a) Full scale, (b) The enlargement. | 119 |
| Figure 7.10: | The Raman spectra of different samples: (a) Full spectra, and (b) zoom in area of 500 to 600 $cm^{-1}$. | 121 |
| Figure 7.11: | SEM images show the morphology of the surface (non Pt coated area) and Pt contact layer of the samples. | 124 |
| Figure 7.12: | The AFM measurements of Pt contact layer on different samples. (a) as grown sample, (b) annealed sample, (c) annealed and cryogenic sample, and (d) porous sample. | 125 |
| Figure 7.13: | The I-V characteristics of different samples under different treatments. | 126 |
| Figure 8.1: | The I-V characteristics of gas sensors operating at (a) room temperature, and (b) 100°C. | 133 |
| Figure 8.2: | The on-off responses of the sensors measured at 25°C and 100°C at a constant voltage of 2V. | 135 |
| Figure 8.3: | SEM image of Pt contact deposited on (a) porous GaN, and (b) as-grown GaN. | 137 |
| Figure 8.4: | The I-V characteristics of as-grown and porous GaN photodetectors. | 139 |
| Figure 8.5: | The I-V characteristics of the various sets of samples with Schottky of (a) Ag on non-porous GaN (b) Ti on non-porous, and (c) Ag on porous GaN; under three different probing conditions. | 143 |
| Figure 8.6: | The change of emission color under different applied voltages when both Schottky contacts were probed as anode and cathode. | 145 |
| Figure 8.7: | Strong blue emission produced by GaN p-n homojunction structures. (a) Sample processed by dry etching using ICP, and (b) sample processed by chemical wet etching. | 147 |
| Figure 8.8: | The I-V characteristics of the GaN p-n homojunction from different workers. (i) Our LEDs; Sample A processed by dry etching only, sample B processed by dry etching and followed with chemical wet etching. Inset shows the enlargement of I-V characteristic of sample B. (ii) Amano's work, and (iii) Kelly's work. | 148 |
| Figure 8.9: | SEM images showing the surface morphology.(a) Sample A, processed by dry etching, and (b) sample B, processed by chemical wet etching. | 149 |

## LIST OF SYMBOLS

| | |
|---|---|
| $a$ | Lattice constant |
| A | Area |
| A** | Richardson's constant |
| $B$ | Magnetic field strength |
| $c$ | Lattice constant |
| $d$ | Distance |
| $d_{hkl}$ | Interplanar spacing of the crystal planes |
| $E_F$ | Fermi level of semiconductor |
| $E_g$ | Band gap |
| $E_v$ | Valence band edge |
| $E$ | Electric field |
| $F$ | Force |
| $h$ | Planck's constant |
| $(hkil)$ | Miller-Bravais indices |
| $I$ | Current |
| $I_o$ | Saturation current |
| $k$ | Boltzmann's constant |
| $l_i$ | Spacing between contacts |
| $L_t$ | Transfer length |
| $m_o$ | Electron mass |
| $m^*$ | Effective mass |
| $m_n$ | Electron effective mass |
| $m_p$ | Hole effective mass |
| $N_D$ | Donor concentration |
| $N_A$ | Acceptor concentration |
| $N_i$ | Number of sites (dipole moment) per area at the interface |
| $n$ | Refractive index |
| $n$ | ideality factor |
| $n$ | Free electron concentration |
| $n$ | Order of diffraction |
| $p$ | Free hole concentration |
| $q$ | Electron charge |
| r | Hall scattering factor |
| $R$ | Resistance |
| $R_H$ | Hall coefficient |
| $Rc$ | Contact resistance |
| $R_{sh}$ | Sheet resistance |
| $R_{sk}$ | Sheet resistance under contact |
| $S$ | Sensitivity |
| $t$ | Thickness |
| $T$ | Absolute temperature |
| $V$ | Voltage |
| $V_D$ | Diffusion voltage |
| $V_H$ | Hall voltage |
| $\Delta V$ | Electrical polarization |
| $w$ | Width |
| $W_C$ | Width of the pad |

| | |
|---|---|
| $W_D$ | Depletion layer width |
| $\alpha$ | Absorption coefficient |
| $\varepsilon$ | Dielectric permittivity |
| $\varepsilon_o$ | Absolute dielectric constant |
| $\varepsilon_r$ | Relative dielectric constant |
| $\sigma$ | Conductivity |
| $\nu$ | Frequency |
| $\theta_i$ | Hydrogen atoms coverage at the interface |
| $\theta$ | Incident / Diffraction angle |
| $\chi$ | Semiconductor electron affinity |
| $\Phi_B$ | Schottky barrier height |
| $\phi_M$ | Metal work function |
| $\phi_S$ | Semiconductor work function |
| $\mu_n$ | Electron mobility |
| $\mu_p$ | Hole mobility |
| $\mu$ | Carrier mobility |
| $\mu$ | Effective dipole moment |
| $\rho$ | Resistivity |
| $\rho_c$ | Specific contact resistivity |
| $\rho_s$ | Sheet resistivity |
| $\infty$ | Infinity |
| $\omega$ | Photon frequency |
| $\lambda$ | Wavelength |

## LIST OF MAJOR ABBREVIATIONS

| | |
|---|---|
| AFM | Atomic force microscope |
| a.u. | Arbitrary unit |
| CTLM | Circular TLM |
| CRT | Cathode-ray tube |
| DAP | Donor-acceptor pair |
| DBE | Donor bound exciton |
| DC | Direct current |
| ECR | Electron cyclotron resonance |
| EDX | Energy Dispersive X-ray |
| ELDs | Electroluminescent devices |
| ELO | Epitaxial Lateral Overgrowth |
| FE | Field Emission |
| FET | Field Effect Transistor |
| FWHM | Full width at half maximum |
| HBT | Heterojunction Bipolar Transistor |
| HCl | Hydrochloric |
| HEMT | High Electron Mobility Transistor |
| HF | Hydrofluoric |
| HVPE | Hydride vapor phase epitaxy |
| ICP | Inductively coupled plasma |
| I-V | Current-Voltage |
| LD | Laser Diode |
| LED | Light Emitting Diode |
| LEEBI | Low–Energy Electron Beam Irradiation |
| LO | Longitudinal optical |
| M | Metal |
| MBE | Molecular Beam Epitaxial |
| MESFET | Metal-Semiconductor FET |
| MIS | Metal-Insulator-Semiconductor |
| MOCVD | Metalorganic vapor deposition |
| MOSFET | Metal-Oxide-Semiconductor FET |
| MS | Metal Semiconductor |
| MSM | Metal Semiconductor Metal |
| OMVPE | Same as MOCVD |
| O.T | Optical transmission |
| PA-MOCVD | Plasma assisted MOCVD |
| PC | Photocurrent |
| PEC | Photoelectrochemical |
| PL | Photoluminscence |
| RF | Radio frequency |
| RHEED | Reflection high energy electron diffraction |
| RGA | Residual gas analysis |
| RGB | Red, green, blue |
| RIE | Reactive ion etching |
| RL | Red luminescence |
| RMS | Root mean square |
| SBH | Schottky barrier height |
| SC | Semiconductor |
| sccm | Standard cubic centimeters per minute |
| SCR | Specific contact resistivity |
| SEM | Scanning electron microscope |

| | |
|---|---|
| SFM | Scanning force microscope |
| slpm | Standard litre per minute |
| TE | Thermionic emission |
| TEM | Transmission electron microscopy |
| TFE | Thermionic field emission |
| TLM | Transmission line model |
| TMAl/TMA | Trimethylaluminum |
| TMGa/TMG | Trimethylgallium |
| TMIn/TMI | Trimethylindium |
| TO | Transverse optical |
| UHV | Ultra high vacuum |
| UV | Ultra Violet |
| VBM | Valence-band maximum |
| XRD | X-ray Diffraction |
| YL | Yellow luminescence |

## KAJIAN KE ATAS BAHAN GaN UNTUK APLIKASI PERANTI

## ABSTRAK

Dalam projek ini, tumpuan kerja adalah pada kajian kualiti bahan GaN yang ditumbuh oleh teknik-teknik yang berlainan, sentuhan logam pada bahan-bahan GaN dan juga kajian pada sifat-sifat asas bahan GaN berliang, serta fabrikasi peranti berasaskan bahan GaN berliang.

Pencirian terperinci untuk mengkaji kualiti bahan GaN yang ditumbuhkan oleh dua teknik berlainan, iaitu, pemendapan wap kimia logam-organik pada tekanan rendah (LP-MOCVD) dan pemendapan wap kimia logam-organik bantuan plasma (PA-MOCVD) telah dijalankan. Selain daripada lapisan penimbal didapati mempengaruhi sifat-sifat fizikal bahan GaN dalam LP-MOCVD, adalah juga didapati bahawa hidrogenasi boleh menghasilkan filem GaN epitaksi pada suhu yang rendah dalam PA-MOCVD.

Pelbagai sentuhan logam pada bahan GaN telah dikaji dalam projek ini. Pt didapati mempunyai sifat elektrik dan kestabilan termal yang terbaik pada suhu tinggi diantara logam-logam sentuh pada n-GaN. Sentuhan ohmik dwi-lapisan Ni/Ag yang baru pada p-GaN telah dikaji, kerintangan sentuh spesifik (SCR) skema dwi-lapisan ini didapati peka pada perubahan suhu dan masa penyepuhlindapan. Selain itu, kajian sentuhan Schottky berdasarkan kepada empat jenis skema logam, iaitu, Ti, Ag, Ti/Ag dan Ag/Ti juga dilakukan pada p-GaN, dan rawatan termal didapati boleh meningkatkan sifat-sifat elektrik bagi sentuhan Schottky secara amnya.

Memandangkan GaN berliang adalah bahan yang baru, ciri-cirinya jarang didapati dalam tinjauan bacaan. Dalam projek ini, pelbagai alat pencirian telah digunakan untuk mengkaji sifat-sifat struktur, morfologi dan optik bahan GaN berliang yang dihasilkan oleh teknik punaran elektro-kimia dengan bantuan sinaran ultra ungu dan teknik punaran tanpa elektro dengan bantuan Pt. Secara umumnya, kajian menunjukkan, sifat-sifat fizikal GaN dapat dipengaruhi oleh lapisan berliang ini. Pada

keseluruhannya, sampel berliang yang dihasilkan oleh dua cara ini didapati mempunyai sifat-sifat yang serupa, akan tetapi, sifat-sifat yang berlainan juga diperhatikan pada bahagian-bahagian tertentu. Selain daripada itu, kajian juga menunjukan GaN berliang yang disebabkan rawatan kimia ini dapat meningkatkan sifat-sifat elektrik sentuhan Schottky Pt pada GaN di mana ketinggian sawar Schottky (SBH) dan kebocoran arus dapat diperbaiki.

Empat peranti GaN berliang telah difabrikasikan. Kecekapan pengesan gas dapat ditingkatkan dengan penggunaan lapisan GaN berliang. Pengesan foto berasaskan lapisan GaN berliang juga menunjukkan potensinya, di mana, arus gelap yang rendah, dan nisbah arus foto kepada arus gelap yang tinggi dapat diperhatikan. Walaubagaimanapun, bagi diod Schottky pemancar cahaya yang dibuat pada p-GaN yang normal, pertukaran warna cahaya dari kuning, hijau ke ungu dapati diperhatikan semasa keupayaan di antara elektrod ditambahkan secara perlahan-lahan, sebaliknya, bagi sampel GaN berliang, hanya cahaya warna biru dapat diperhatikan. Selain daripada itu, penggunaan GaN berliang dalam struktur diod pemancar cahaya (LED) homo simpangan p-n tidak dapat meningkatkan kecekapannya, di mana voltan ambang yang agak tinggi dihasilkan bagi sampel berliang jika dibandingkan dengan sampel asas. Semua kajian permulaan ini menunjukkan bahawa lapisan GaN berliang ini berpotensi untuk meningkatkan prestasi peranti pengesan, tetapi, ianya belum lagi dapat dibuktikan and dikaji sepenuhnya bila ia digunakan pada peranti pemancar cahaya.

# THE STUDY OF GaN MATERIALS FOR DEVICE APPLICATIONS

## ABSTRACT

In this project, works are focusing on the investigation of the material quality grown by different techniques, metal contacts on GaN materials as well as the study of the fundamental properties of the porous GaN materials and the fabrication of devices based on porous GaN materials.

Detailed characterizations for the investigation on the GaN films quality grown by two different techniques, i.e. low pressure metal-organic chemical deposition (LP-MOCVD) and plasma assisted MOCVD (PA-MOCVD) have been carried out. Apart from buffer layer was observed to be able to influence the physical properties of GaN films in LP-MOCVD, it is also found that in PA-MOCVD, hydrogenation during growth was capable of producing epitaxial GaN films at reduced temperatures.

Various metal contacts on GaN materials have been investigated in this project. Pt was found to have excellent electrical properties and thermal stability at elevated temperatures among the metal contacts on n-GaN. A new Ni/Ag bi-layer ohmic contact on p-GaN has been explored; the specific contact resistivities (SCRs) of this bi-layer scheme were observed to be sensitive to the change of annealing temperatures and durations. Other than that, the study of Schottky contacts based on four different metallization schemes i.e. Ti, Ag, Ti/Ag, and Ag/Ti were also performed on p-GaN, and heat treatment was found to be able to improve the electrical properties of Schottky contacts generally.

Since porous GaN is a new form of material, the properties are scarcely found in the literature. In this project, various characterization tools have been used to investigate the structural, morphological and optical properties of porous GaN generated by ultra-violet assisted electrochemical etching and Pt assisted electroless etching methods. Generally, the studies showed that the physical characteristics of the GaN were found to be influenced significantly by the porous layer. Overall the porous

samples produced by these two techniques were found to have many similarities, however, different characteristics were also observed in certain areas. Other than that, study also showed that chemical treatment induced porous GaN layer was able to enhance the electrical properties of Pt Schottky contacts on GaN in which the Schottky barrier height (SBH) and leakage current were improved significantly.

Four devices have been fabricated from porous GaN. Performance of the gas sensor was found to be enhanced substantially by using porous GaN layer. Photodetector fabricated from porous GaN layer also showed promise in which low dark current and higher photo-current to dark current ratio were observed. On the other hand, for light emitting Schottky diodes fabricated from as-grown p-GaN, the change of emission colors from yellow, green to violet was observed when the potential between the electrodes was increased gradually, however, there was only blue emission observed when electrical bias was applied on the porous GaN sample. In addition, the use of porous GaN layer in p-n homojunction LED structure shows no improvement on the device performance, since relatively high turn on voltage was produced for the porous sample as compared to as-grown sample. All these initial studies reveal that porous GaN layer has the potential for the substantial improvement of the performance of sensing devices. However, the potential of porous GaN layer has not been fully proven and explored when it is applied in the light emitting devices.

# CHAPTER 1
# INTRODUCTION

## 1.1 Introduction to III-nitrides

The III-V nitrides have long been viewed as a promising system for semiconductor devices operating in the blue and ultra-violet spectra region. In III-V nitrides family, AlN, GaN, InN and their alloys are all wide bandgap semiconductor materials, and can crystallize in both wurtzite and zinc-blende polytypes. The wurtzite polytypes of GaN, AlN and InN form a continuous alloy system whose direct bandgap cover from 1.9 eV for InN, to 3.4 eV for GaN, to 6.2 eV for AlN. Following recent studies, the InN bandgap was found to be smaller than 0.8 eV (Wu *et al.*, 2002, Saito *et al.*, 2002). These findings further span the whole nitrides bandgap from infra-red into deep ultra-violet (UV) regions. This makes the nitride system attractive for optoelectronic device applications, such as light emitting diodes (LEDs), laser diodes (LDs) and photodetectors.

High temperature/high power/high frequency electronics is another area receiving enormous attention for III-V nitrides (Pearton *et al.*, 2000). Presently, Si and GaAs are the two most widely used materials in the semiconductor industries. Electronics devices based on current Si and GaAs semiconductor technologies are not able to operate at elevated temperatures due to the uncontrolled generation of intrinsic carriers. On the other hand, the wide bandgap nature of nitrides such as GaN is attractive for high temperature applications, because their intrinsic properties are maintained at much higher temperatures. This suggests that GaN-based power devices can operate with less cooling and fewer high cost processing steps associated with complicated structures designed to maximize heat extraction. In addition, the III-V nitrides posses higher breakdown electric field which sustains larger voltage gradient, enabling thinner active regions, lower on resistances and high voltage operation as well as high electron drift velocity which leads to faster operating speed.

Other superior properties of nitrides include large piezoelectric constants and possibility of passivation by forming thin layers of $Ga_2O_3$ or $Al_2O_3$ as well as high bonding energy. GaN has a bond energy of 8.92 eV/atom, InN 7.72 eV/atom, and AlN 11.52 eV/atom; giving high mechanical strength, chemical inertness and radiation resistance (Pearton, *et al* 1999). Moreover, nitride materials are non-toxic, environmentally friendly materials compared to other conventional III-V compounds such as GaAs and GaP which contain arsenic and phosphorous, and therefore are toxic for human.

Researchers have laboured for more than 35 years and have been able to determine many of the physical parameters and properties of the III-V nitride semiconductors. Among all the nitride semiconductors, GaN is by far the most heavily studied. Table in Appendix I summarizes the fundamental properties of wurtzite III-nitride semiconductors at room temperature.

## 1. 2 Historical development of Nitrides

The evolution of nitride semiconductors has been interesting and followed a bumpy road. GaN was first synthesized by Johnson (Johnson, *et al* 1932) in 1932, in which ammonia was passed over hot gallium. This technique produced small needles and platelets. Grimmeiss (Grimmeiss, et al. 1959) used similar method to produce small GaN crystal for the purpose of measuring photoluminescence spectra. In 1969, Maruska and Tietjen (Maruska and Tietjen, 1969) succeeded in growing the first single-crystal GaN on a sapphire substrate by using hydride vapor phase epitaxy (HVPE) technique. They found that GaN posseses a direct transition band structure with bandgap energy of about 3.39 eV.

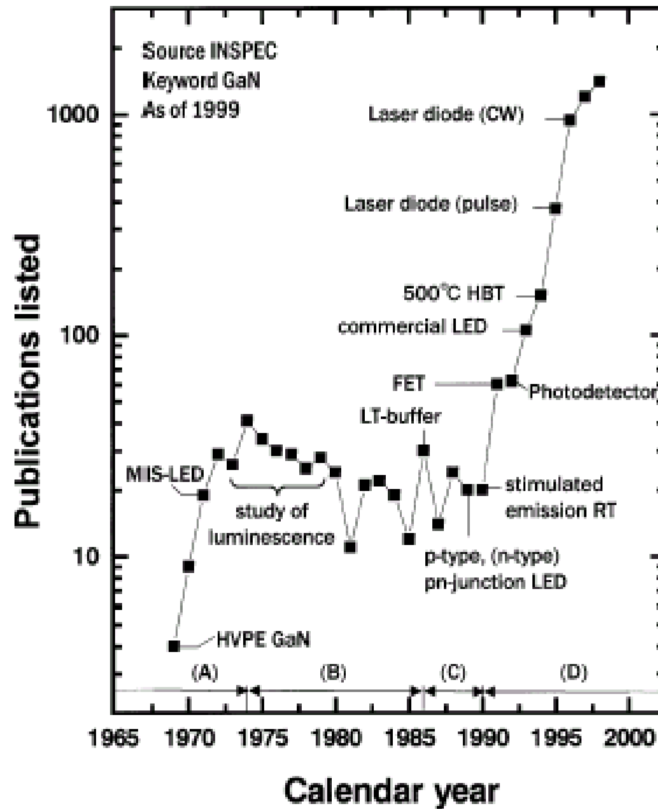


Fig. 1.1 Number of publications (INSPEC) and activities in GaN over the years (adapted from Akasaki, 2002)

The accomplishment of Maruska and Tietjen accelerated and inspired the research on GaN, particularly the fabrication of the Zn-doped first blue LED by Pankove (Pankove, *et al* 1972). This was a metal-insulator-semiconductor (MIS) structured device. The unintentionally-doped GaN produced at that time was strongly n-type with high residual electron concentration which was believed to be due to nitrogen vacancies. However, the failure in achieving the p-type doping has resulted in many researchers withdrawing from the field of research on the nitride semiconductors, subsequently led to slow GaN research activities, and this started a big gap in the history of the nitrides as indicated in Fig. 1.1 which shows the number of publications (INSPEC) and research activities in nitrides over the years.

It was the perseverance of Akasaki that eventually paid off in the pursuit of the p-type GaN conduction. In 1985, Akasaki with Amano and Hiramatsu developed organo metallic vapor phase epitaxy (OMVPE) for the nitride growth and low-

temperature AlN buffer layers. Now the low temperature buffer layer becomes part of the growth process before the main epitaxial layer is grown onto it. This low temperature buffer layer lowered the large background electron concentrations from previous $10^{19}$ – $10^{20}$ $cm^{-3}$ levels to $10^{17}$ $cm^{-3}$, which not only improved the crystal quality but set the stage for p-type doping. In fact, the p-type conduction was an accidental discovery. In 1988, Amano (Amano, *et al* 1988) was observing the cathodoluminescence of GaN:Mg under scanning electron microscopy (SEM) and noticed that the brightness increased with further raster scanning. Low–energy electron beam irradiation (LEEBI) treatment of the sample showed that the luminescence efficiency had increased two orders of magnitude. This surprising phenomenon was explained by Van Vechten (Van Vechten, *et al* 1992), who proposed that the shallow acceptor level of Mg was compensated by a hydrogen atom complexing with the Mg acceptor. The energy of the electron beam releases the hydrogen atom from the complex that then becomes a shallow acceptor about 0.16 eV above the valence band. The follow-up investigation of Nakamura (Nakamura, *et al* 1992) found out that thermal annealing GaN:Mg above 750°C in $N_2$ or vacuum also converted the material to conducting p-type. Since then the research activities on GaN have increased tremendously.

## 1.3 Research Background

In recent years, the miniaturization of electronic devices has been drastically enforced in the semiconductor technology. Knowledge on the microscopic electronic properties of thin film becomes very important. On the other hand, the crystalline microstructure is a fundamental property of the semiconductor. The microstructure is closely related to the growth condition, it has a significant influence on the quality of the film and the performance of the electronics devices eventually. The detailed characterizations will be able to provide useful information about the quality of the GaN films, so that some precautions can be employed during the growth of the GaN and

groundwork therefore is laid to optimize the growth conditions, which will lead to improvement of the quality of the films.

GaN-based materials have been investigated intensively in recent years due to their potential applications in visible and UV LEDs and LDs for lighting and data storage, field effect transistors (FETs) for high-temperature and high-power electronics devices, and solar-blind UV detectors (Liu and Lau, 1998). These exciting applications present numerous challenges in making high quality metal contacts to GaN-based materials, which is crucial for device performances. Generally, making low-resistance ohmic contacts is difficult for GaN-based materials, particularly p-type GaN due to difficulty in doping. This difficulty has been one of the major obstacles in fabricating highly efficient LED and LDs. Moreover, conventional metallization schemes may not have the adequate thermal stability when devices operate at high power and high temperature environments (Liu and Lau, 1998).

Porous semiconductors have drawn great deal of attention in recent years, primarily due to the potential for intentional engineering of properties not readily obtained in the corresponding crystalline precursors as well as the potential applications in chemical and biochemical sensing. Porous semiconductors are also under study as possible templates for epitaxial growth (Inoki, *et al* 2003, Ponce and Bour, 1997), in which the pores could act as sinks for mismatch dislocations and accommodate elastic strain in heterostructures, this eventually leads to the growth of high quality epitaxial films with low structural defect density and strain.

Interest in porous semiconductors also arises from the potential applications in optoelectronics area. Porous semiconductors have been demonstrated to be capable of shifting the emission wavelength and enhancing the luminescence efficiency as compared to the unetched precursors (Fauchet, *et al* 1995, Chattopadhyay, *et al* 2002). Among porous semiconductors, porous silicon receives enormous attention and has been investigated most intensively. However, the instability of the physical properties has prevented it from large scale application. This leads to the development of other

porous semiconductors, for instances, the conventional III-V compounds such as GaAs, GaP and InP, however, low band gap semiconductors always suffer from the generation of charge carriers due to undesirable background optical or thermal excitation. The research in porous GaN is strongly driven by the wide band gap and superior physical properties such as the excellent thermal, mechanical and chemical stability, nevertheless, the study of porous GaN is still in the stage of infancy. Since porous GaN is a new form of material, most of the fundamental properties are not available in the literature, furthermore, there is no device fabricated based on porous GaN reported in the literature, therefore there is a big room for the exploration of porous GaN.

## 1.4 Research Objectives

In this project, the research mainly focuses on the investigation of the GaN-based materials for device applications. The project starts with the detailed study of the material quality grown by two different techniques, i.e. low pressure metal organic chemical vapor deposition (LP-MOCVD) and plasma-assisted metal organic chemical vapor deposition (PA-MOCVD). This investigation provides the fundamental study of the characteristics of the GaN films, subsequently; it allows a better understanding of the material quality for the study of porous GaN.

In this work, a wide variety of metal contacts on n- and p-GaN materials have been investigated under different conditions, i.e. effect of thermal treatments and wide range of annealing temperatures, for the study of the change of electrical, morphological properties and thermal stability of the contacts under different environments. Attention is specially paid to metal contacts on p-type GaN materials. Since metal contacts to p-GaN are relatively less investigated as compared to n-GaN, this allows us to exploit many new research areas on p-GaN, for instance, novel metallization scheme, i.e. Ni/Ag. These metallization schemes eventually will be applied in the fabrication of various devices.

The studies of material quality of GaN films and metal contacts on GaN-based materials are two important research areas which will give an insight in the GaN technology, this eventually provides a better understanding on the fundamental properties for the subsequent study of the porous GaN materials and device fabrication.

Following the intensive investigations of material quality and metal contacts, tremendous effort is also channeled into the exploration the fundamental properties of the porous GaN materials; a new form of material which is rarely reported in the literature, therefore, in this project, works have been devoted to the study of the structural, morphological, optical and electrical properties of this material. Apart from that, the devices, i.e. gas sensor, MSM photodetector, light emitting Schottky diode and light emitting diode based on porous GaN are also fabricated and compared to other non-porous-based devices so that the potential of porous GaN could be fully explored. The ease of fabrication, simple experimental setup and the availability of characterization tools for measuring the performance of the devices are the reasons for choosing these devices in this project.

### 1.4.1 Originality of the research works

A number of original works have been carried out in this project. For instances, the investigation of new metallization scheme Ni/Ag ohmic contacts on p-type GaN; and the study of light emitting Schottky diodes based on p-GaN. For the porous GaN material aspects, the use of porous GaN layer for improving the electrical characteristics of Pt Schottky contacts; and the fabrication and investigation of various devices based on porous GaN layer in this project, i.e. gas sensor, metal-semiconductor-metal (MSM) photodetector, and LED have not been reported in the literature. In addition, a much simpler electroless etching technique for obtaining porous GaN has also been developed during the course of this project.

### 1.5 Outline of the Thesis

The content of this thesis is organized as follows:-

Chapter 2 encompasses an overview of the GaN technology, such as the nitride epitaxial growth techniques, factors influencing the crystalline quality of GaN, metal-GaN contact technology, as well as the development of porous GaN. The basic principles of characterization tools, process equipment, and devices, the theory of metal-semiconductor contact, porous GaN formation mechanisms as well as the basic principles of some devices (which have been fabricated in this project) are covered in Chapter 3. Methods in studying material properties, metal contacts, porous GaN as well as the fabrication and characterization of various types of devices are presented in Chapter 4. The results obtained from the research works are then analyzed, discussed in Chapter 5, 6, 7 and 8. Chapter 5 and 6 are devoted to the study of GaN material quality and metal contacts on GaN. Chapter 7 is focusing on the study of the properties of the porous GaN, whereas Chapter 8 reports on the performance of the devices fabricated based on porous GaN. In the final Chapter 9, the conclusion of the thesis with a summary of the research work is presented. A few suggestions for future research are also included.

# CHAPTER 2
# LITERATURE REVIEW

## 2.1 Introduction

In this chapter, a brief overview of GaN technology is presented. The review mainly focuses on the nitride semiconductors growth techniques, factors influencing the GaN crystalline quality, metal-GaN contact technology and the development of the porous GaN.

## 2.2 Nitride Epitaxial Growth Techniques

Tremendous efforts have been applied to the epitaxial growth of III-V nitride materials. Most of the works so far can be divided into three categories: hydride vapor phase epitaxy (HVPE), metalorganic chemical vapor deposition (MOCVD), and molecular beam epitaxy (MBE) methods.

### 2.2.1 Hydride Vapor Phase Epitaxy (HVPE)

In the early investigation of III-V nitrides, HVPE was the most successful epitaxial growth technique to grow GaN thin films which was developed by Maruska and Tietjen in 1969. In their method, HCl vapor flowing over a Ga melt, cause the formation of GaCl which was transported downstream. At the substrate, GaCl mixed with $NH_3$ leads to the chemical reaction:

$$GaCl + NH_3 \rightarrow GaN + HCl + H_2$$

The growth rate was quite high (0.5μm/min) which allowed the growth of extremely thick film and the properties were relatively not influenced by the thermal and lattice mismatches with the substrate. Zn or Mg dopant incorporation could be achieved by simultaneous evaporation of dopant source in the HCl stream.

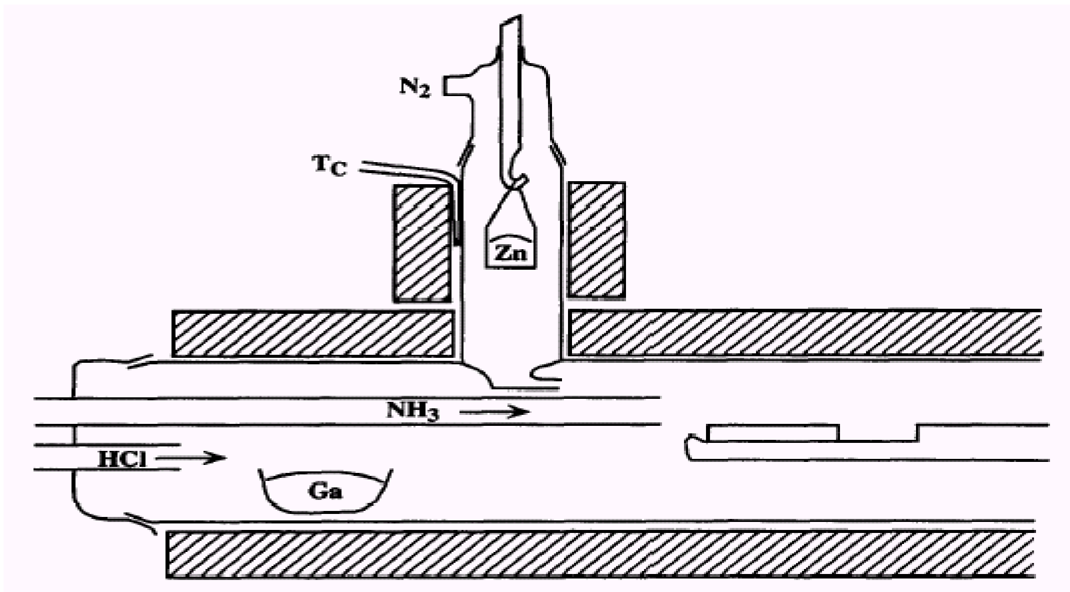


Fig. 2.1 Schematic diagram of a vapor transport GaN growth reactor (adapted from Pankove, 1973).

The early GaN grown by this technique had very high background n-type carrier density, typically~$10^{19}cm^{-3}$. Fig. 2.1 shows the schematic diagram of the HVPE growth reactor.

### 2.2.2 Metalorganic Chemical Vapour Deposition (MOCVD)

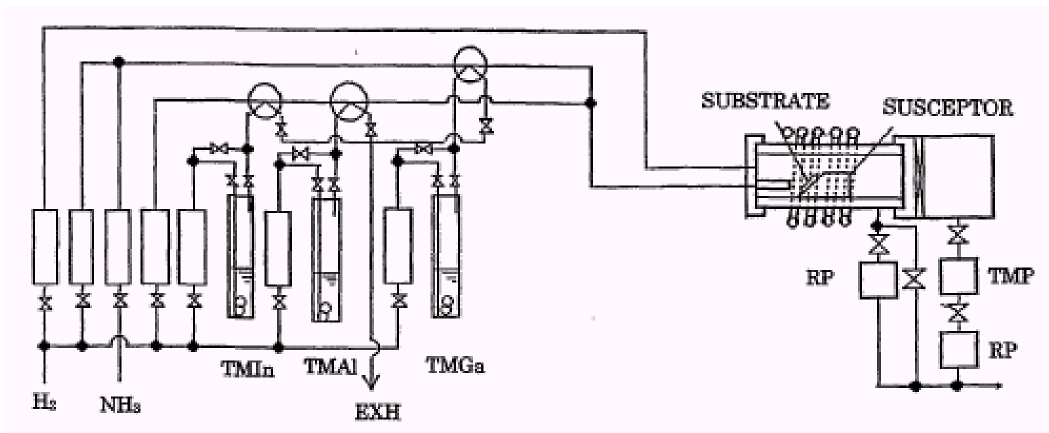


Fig. 2.2 The schematic diagram of a typical MOCVD growth reactor (adapted from Akasaki and Amano 1997)

Presently, MOCVD is the most successful and widely used technique for growing nitride materials. It involves the transport of vapours of metal organic compound in a carrier gas with thermal decomposition at or near the substrate. Fig. 2.2 shows the schematic diagram of a typical MOCVD.

The general popularity of the MOCVD arises in part from its scalability to production volumes of high quality multilayer heterostructures. However, the high growth temperatures, necessary for efficient decomposition of the precursors, may influence the quality of the grown heterostuctures through thermal diffusion, with large thermal expansion differentials introducing additional dislocation. Therefore, many attempts have been made to reduce the MOCVD growth temperature by providing additional, non-thermal, decomposition routes (Tansley *et al* 1997). Many improved versions have been developed since the introduction of this growth technique.

#### 2.2.2.1 Atmospheric pressure MOCVD

In conventional atmospheric pressure MOCVD reactor, III precursors used for the growth of nitride materials come from metal-organic source i.e. trimethylgallium (TMGa/TMG), trimethylaluminum (TMAl/TMA), or trimethylindium (TMIn/TMI). In the case of GaN growth, TMGa reacts with nitrogen in the form of $NH_3$ which requires high temperatures (typically 1000°C) to become reactive, and need to be abundant, so that the III/V ratio is very small. This causes technical difficulties in flow rate control, mixing and reactant flows over substrate (Tansley et al 1997). In view of technical difficulties, Nakamura *et al* (1991) designed a two-flow MOCVD reactor specifically for nitride growth which has been highly successful. In this reactor, the main flow carries the reactant gas parallel to the substrate. The second subflow perpendicular to the substrate forces, on the other hand, a deviation of the reactant gas toward the substrate, and suppress thermal convection effects. A rotating susceptor was used to enhance uniformity of the deposited films. The key aspect of this design is a downward

subflow of $H_2$ and $N_2$ which has been claimed to improve the interaction of the reactant gasses with the substrate. Fig. 2.3 shows the schematic diagram of the reactor.

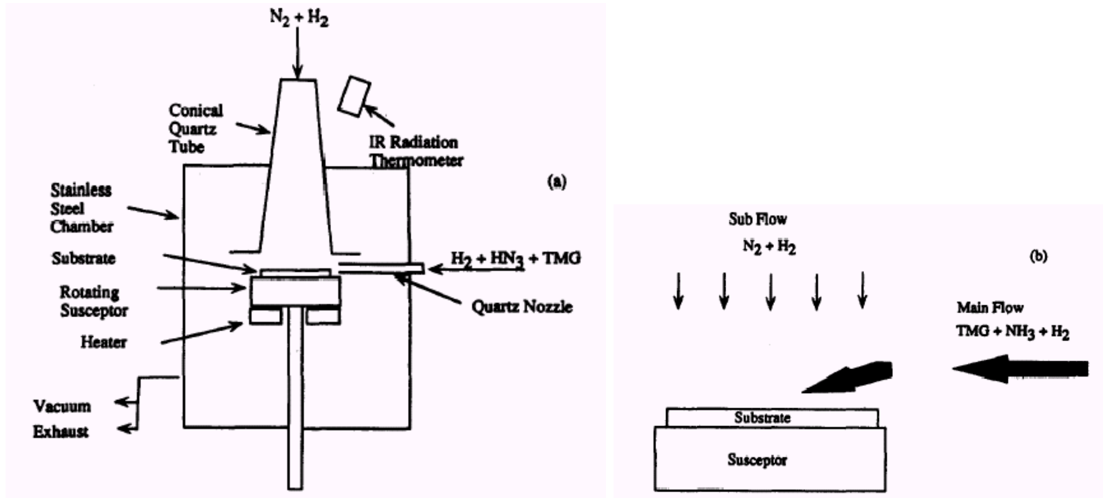


Fig. 2.3 The schematic diagram of the two-flow MOCVD reactor (adapted from Nakamura *et al* 1991).

### 2.2.2.2 Low pressure MOCVD (LP-MOCVD)

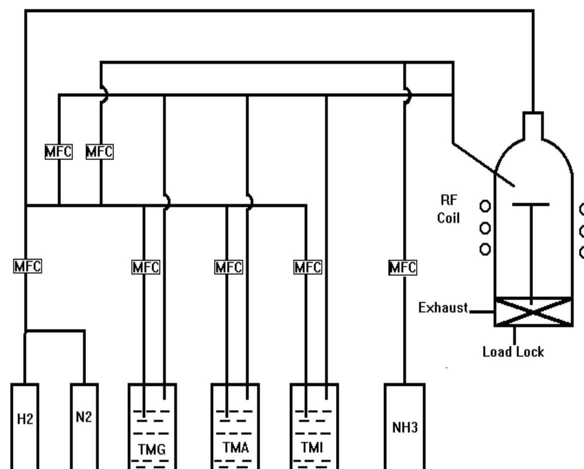


Fig. 2.4 The schematic diagram of the commercial vertical rotating disk LP-MOCVD reactor (adapted from Hassan and Kordesch, 2000)

LPMOCVD has been developed for the purpose of realizing growth of GaN at lower temperature. At low pressure, the decomposition products have a lower collision frequency, so that a higher proportion of "unrecombined" radicals arrive at the growth surface. Heat of formation liberated at the surface provides the mobility necessary for

the adsorbates to diffuse to nucleation sites with a reduced requirement for kinetic energy to be provided by a hot substrate, making growth possible (Tansley *et al* 1997). Fig. 2.4 shows the commercial vertical rotating disk LP-MOCVD reactor.

### 2.2.2.3 Plasma-assisted MOCVD (PA-MOCVD)

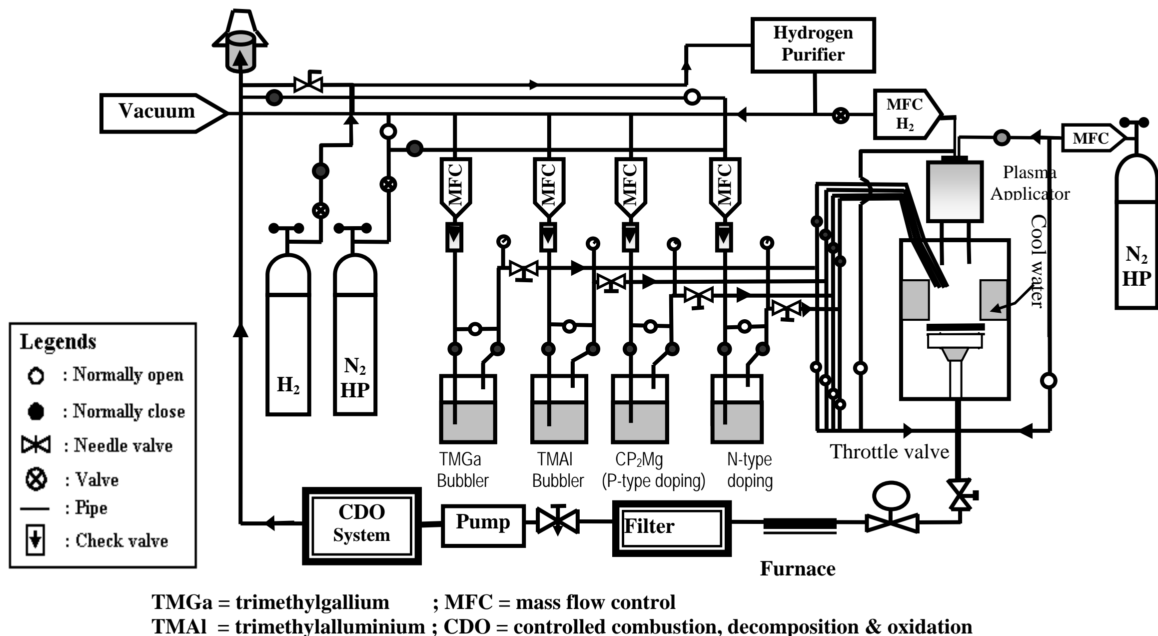


Fig. 2.5 The schematic diagram of plasma-assisted MOCVD reactor (The schematic diagram provided by Prof. Barmawi, of ITB)

Fig.2.5 shows the schematic diagram of the reactor. It consists of a water-cooled stainless-steel vertical reactor which is equipped with a plasma-cracking cell. The reactor was pumped by a combination of a root blower pump and a rotary vacuum pump. A low power downstream plasma cavity (ASTex) supplied the reactive N-plasma from nitrogen gas and reactive H-plasma from hydrogen gas. The plasma is generated by 2.45 GHz microwave at power ranges from 200 to 250 Watt, and the un-cracked TMGa and plasma-cracked $N_2$ gas were used as the Ga and N sources. The $H_2$ carrier gas was purified by passing through a heated palladium cell. The growth temperature was monitored by a thermocouple inserted inside the heater.

The development of PA-MOCVD is strongly driven by the need to reduce the growth temperature. A typical MOCVD reactor requires high growth temperature (above 1000°C) which is necessary for the efficient decomposition of the nitrogen precursor and this may influence the quality of heteroepitaxial grown GaN films, with large thermal expansion differentials, thus introducing high densities of structural defects (Tansley *et al* 1997)

### 2.2.3 Molecular Beam Epitaxy (MBE)

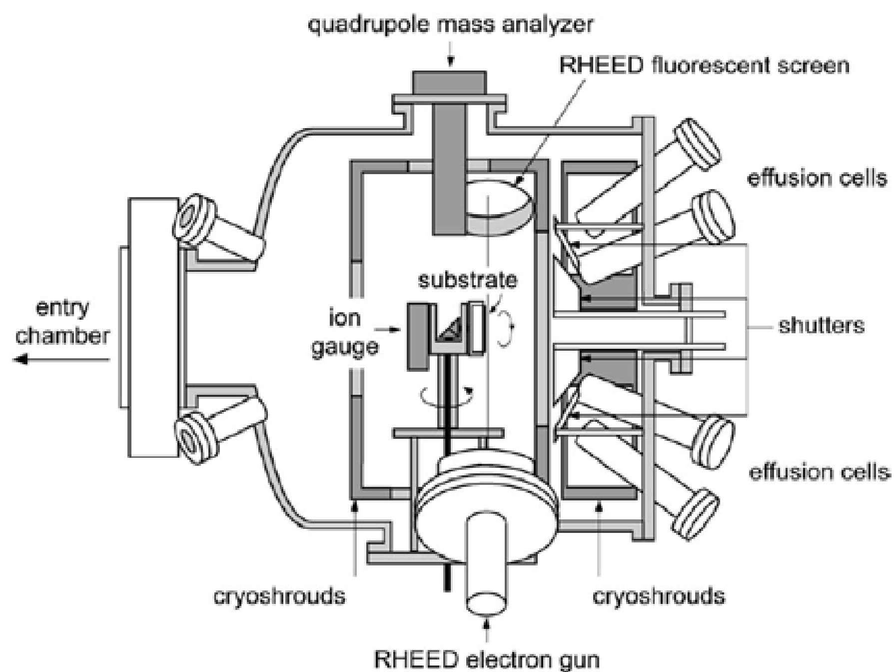


Fig. 2.6 Schematic diagram of the MBE growth chamber (Adapted from Franchi, *et al* 2003)

MBE was developed in late 1960s by A.Y, Cho. It offers the possibility to grow epitaxial films on crystalline substrate with atomic layer precision. An MBE system can be considered as a refined form of evaporator.

Fig. 2.6 shows the schematic diagram of a typical modern MBE growth chamber. Substrates are loaded into the growth chamber via a vacuum load lock system, so that the chamber is isolated from the air. During the growth process, elemental sources are heated in Knudsen cells and evaporated at controlled rate onto

a heated substrate under ultra-high vacuum (UHV) conditions ~$10^{-10}$ – $10^{-11}$ torr. The UHV growth environment is crucial to the MBE process. It provides an ultra clean growth ambient leading to epitaxial layers with the highest purity. This is extremely important for growing high quality semiconductor materials which are used for high performance devices. Under UHV condition, the long mean-free path of particles minimizes collisions or reactions between molecules in the beam, which results in a line-sight growth reaction at the surface.

Since MBE is a UHV-based technique, it has the advantage of being compatible with wide range of surface analysis techniques. Mass spectrometer for residual gas analysis (RGA) and reflection high energy electron diffraction (RHEED) are two important *in situ* analysis tools which are commonly incorporated in the MBE system to monitor the growth rates and epitaxial film quality during growth process.

GaN film grown by MBE usually carried out at relatively low temperatures of 650 to 800°C with typical growth rate of one to three monolayers per second, approximately 0.3 to 1 μm/hr. On the other hand, molecular nitrogen is stable and inert gas which has a strong N-N bond and does not chemisorb on a GaN surface for temperature below 950°C, Therefore atomic nitrogen or nitrogen molecules with weaker bonds should be supplied. Radio frequency (RF) or electron cyclotron resonance (ECR) plasma sources are commonly employed to activate the nitrogen species.

### 2.2.3.1 MBE growth kinetics

Fig. 2.7 shows the schematic illustration of the surface process in a MBE system. There are a number of processes involved during growth (Herman and Sitter 1996), which can be summarized as:-

(a) Adsorption of the molecules or constituent atoms impinging on the substrate surface,

(b) Surface migration and diffusion of these molecules on the substrate,

(c) Incorporation of the adsorbed species into the grown epilayers or the crystal lattice of the substrate, and

(d) Thermal desorption of atoms not being incorporated into the lattice.

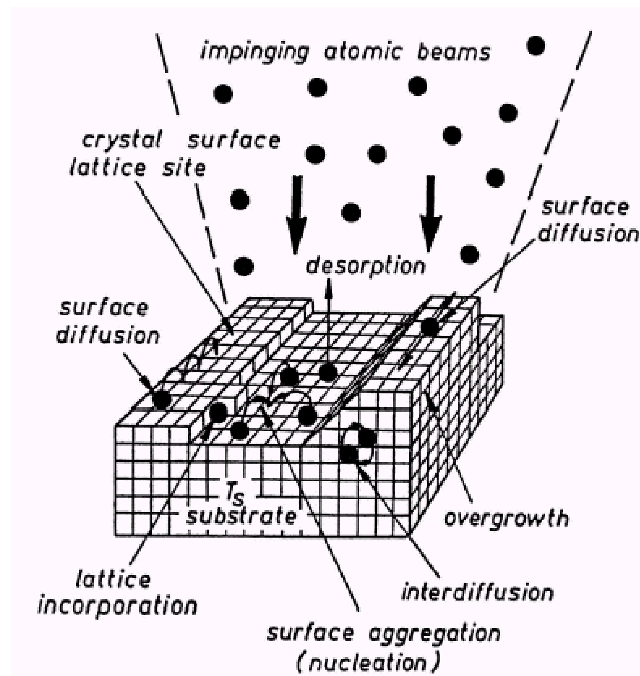


Fig 2.7 Schematic illustration of the surface processes during growth in a MBE system (Adopted from Herman and Sitter 1996)

### 2.2.3.2 The strengths of MBE

Semiconductor compounds fabricated by MBE offers a number of advantages compared to other growth techniques, for instances, the opening or closing of mechanical shutter, located in front of each furnace, allows turning a specific molecular beam on or off instantaneously, resulting in abrupt interfaces in the order of one monolayer. This unique capability provides precise composition and doping profiles, extremely well-defined layer; enable the fabrication of device structures with critical performance. In addition, the consumption of source materials is significantly reduced as compared to MOCVD.

The growth of GaN films by MBE at reduced temperatures not only allow wider range of substrates to be investigated but also reduce the structural defects due to

large thermal expansion differentials. Moreover hydrogen-free environment also provides the growth of p-type Mg-doped GaN without the need for post-growth processing.

## 2.3 Factors Influencing GaN Crystalline Quality

Many fundamental questions about the III-V nitrides growth are still being raised. One of the major problems rests with the absence of well-suited substrates, since GaN single crystals of sufficiently large dimensions are not yet available, therefore GaN film has to be grown heteroepitaxially on foreign substrates, this leads to the generation of high density of structural defects. However, the employment of low temperature buffer layer coupled with the advancement of epitaxial growth techniques allow great enhancement in the crystalline quality and subsequently the reduction of the high background electron density in GaN, these lead to a tremendous improvement of carrier mobility and eventually the performance of GaN-based devices.

### 2.3.1 Substrates

One of the major difficulties which hinders the GaN research is the lack of a substrate material that is lattice matched and thermally compatible with GaN. High dislocation densities arise in GaN epilayers due to the large mismatch between film and substrate, contributing to the low mobility and high residual carrier density. In fact, homoepitaxy is an ideal situation where it is possible to minimize problems associated with difference in lattice, wetting as well as thermal expansion between substrate and film. However, the equilibrium phase relationships between gallium, nitrogen and GaN present formidable technological problems. As a result, the bulk growth must resort to high temperatures of 1400 - 1600°C and extremely high pressure of 12-15 kbar that yield small size (few mm) GaN (Porowski and Grzegory 1997).

Table 2.1 Lattice parameters and thermal expansion coefficient of prospective substrates for nitrides epitaxial growth (Data extracted from Popovici and Morkoc 2000)

| Crystal | Symmetry | Lattice Constant (nm) (a; c) | Thermal Expansion Coef. (a; c) ($\times 10^{-6}K^{-1}$) |
|---|---|---|---|
| GaN | Wurtzite | (0.3189; 0.5185) | (5.59; 3.17) |
| GaN | Cubic | 0.452 | - |
| AlN | Wurtzite | (0.3112; 0.4982) | (4.2; 5.3) |
| InN | Wurtzite | (0.353; 0.569) | |
| Sapphire | Hexagonal | (0.4758; 1.299) | (7.5; 8.5) |
| ZnO | Wurtzite | (0.3250; 0.5213) | (8.25; 4.75) |
| 6H-SiC | Wurtzite | (0.308; 1.512) | (4.2; 4.68) |
| 3C-SiC | Cubic | 0.436 | - |
| Si | Cubic | 0.54301 | (3.59) |
| GaAs | Cubic | 0.56533 | 6 |
| InP | Cubic | 0.5869 | 4.5 |
| MgO | Cubic | 0.4216 | 10.5 |
| MgAlO2 | Cubic | 0.8083 | 7.45 |
| LiAlO2 | Tetragonal | (0.5406; 0.626) | - |
| ScMgAlO4 | Tetrahedral | (0.3240; 2.511) | (6.2; 12.2) |

The density of threading dislocation defects in GaN films is always in the range of $10^{10}cm^{-2}$. These defects originate from the substrate/GaN interface and propagate into the epilayer. The large difference of lattice constant and thermal expansion coefficient between the substrate and GaN is considered to be the major factor attributing to the high density of this defect. Table 2.1 shows the lattice constant and thermal expansion coefficient for some prospective substrates as compared to nitrides. Sapphire exhibits a higher thermal expansion coefficient relative to GaN, and for 6H-SiC, the thermal expansion coefficient is smaller than GaN. GaN films grown on sapphire and 6H-SiC will experience compressive and tensional biaxial strain

respectively (Monemar *et al* 1997). However, with the formation of threading dislocations, the strain in the GaN epilayer will be released.

Although sapphire ($Al_2O_3$) possesses a substantially different lattice constant and thermal expansion coefficient from GaN, it is still the most commonly used substrate for GaN growth because of its wide availability, hexagonal symmetry, and ease of handling and pre-growth cleaning. Sapphire is also stable at high temperature (~1000 °C), which is normally required for GaN film grown by metalorganic chemical vapor deposition (MOCVD) method. On the other hand, sapphire is electrically insulating, therefore, all electrical contacts have to be formed on the front side of the device, reducing the area available for devices and complicating the device fabrication (Liu and Edgar 2002).

Si is another potential substrate due to the low price, high quality and wide availability as well as easy integration with the current silicon technology. Both Si (110) and (111) are employed for wurtzitic GaN growth. However, GaN grown on Si (001) is predominantly cubic (Popovici and Morkoc 2000).

Table 2.2 Lattice mismatch between GaN and the most commonly used substrates

| Substrate | (%)Lattice Mismatched | Reference |
|---|---|---|
| (0001) $Al_2O_3$ | 16 | (Kung *et al* 1994) |
| (0001) 6H-SiC | -4 | (Tansley *et al* 1997) |
| 3C-SiC | -4 | (Tansley *et al* 1997) |
| (100) GaAs | 20 | (Tansley *et al* 1997) |
| (111) GaAs | 20 | (Tansley *et al* 1997) |
| (001) Si | 17 | (Tansley *et al* 1997) |
| (111) Si | 17 | (Tansley *et al* 1997) |

6H-SiC exhibits a closer lattice constant and thermal expansion coefficient to GaN, however, this substrate is very expensive. GaAs has been used as substrate despite its poor compatibility. This is mainly due to its widely availability and familiarity of the researchers. Other uncommon substrates such as MgO, ZnO, $MgAl_2O_4$ (Popovici and Morkoc 2000), also have been used as substrate, however, there are little technical information available in the literature, therefore, the use of these substrates need to be further developed and explored.

Lattice mismatch between GaN and the most commonly used substrates is summarized in Table 2.2.

### 2.3.2 Buffer layer

Since GaN single crystals with practically large dimensions are not yet available, single crystalline film has to be grown heteroepitaxially on substrates which are normally not lattice matched and thermally compatible. Therefore heteroepitaxial growth is accompanied with high density of structural defects such as stacking faults, threading dislocation (Sverdlov *et al* 1995), as well as vacancies and impurities (Meyer *et al* 2000), which form shallow and deep levels inside the band gap and eventually degrade the optical and electrical properties of the films. The major problem in obtaining high quality heteroepitaxial grown GaN film is mainly due to the formation of defects in the nucleation layer which is attributed to the inhomogeneous wetting of the substrate. Therefore direct deposition of GaN on substrates would result in poor crystalline quality of the film.

The introduction of low temperature buffer layer is one of the promising approaches that can reduce the structural defect significantly. AlN is commonly used as a buffer for GaN grown on sapphire. Buffers are amorphous-like structure with small crystallites (Amano *et al* 1988) which are normally deposited at about 600°C with layer thickness between 50 – 100 nm prior to the growth of GaN film. The initial growth stage is very important in obtaining heteroepitaxy and eventually a good quality of the film

(Wang *et al* 1996). The epitaxial growth can be a two-dimensional (2-D): layer-by-layer mode, a three-dimensional (3-D): island mode, or a mixed mode: layer-by-layer plus islands. The first mode would result in the smooth surface, while the last two modes give rough surface and lead to low quality of epitaxial layers. The mode of growth is governed by many factors. For instances, the interfacial energy of the solid and vapor phases, as well as the vapor phase and substrate. This in turn depends on the growth temperature, the bond strength and bond lengths of the substrate and the overgrowth atoms, the rate of species impingement, surface migration rates of reactants, supersaturation of the gas phase, and the size of critical nuclei (Popovici and Morkoc 2000).

There has been reported that GaN films grown with AlN buffer layer have led to two orders of magnitude reduction in background electron while increasing the carrier mobility by a factor of 10, and the near band gap photoluminescence was two orders of magnitude more intense, moreover the x-ray diffraction peak width was four times smaller (Akasaki *et al* 1989). The buffer layer reduces the effect of strain, dislocations and cracking defect in the GaN films on large lattice and thermally-mismatched substrates significantly (Tansley *et al* 1997). The buffer layer not only relaxes the strain in the heteroepitaxial growth but partly blocks the detrimental effect of the substrate, such as the crystallographic orientation of the substrate (Akasaki *et al* 1989). The buffer layer is also thought to play an important role in supplying nucleation centres which have the same orientation as the substrate and promoting the lateral growth of the film due to the decrease in interfacial free energy between the film and the substrate.

## 2.4 Overview of Metal-GaN contact technology

### 2.4.1 Ohmic contact on GaN

As the GaN device technology advances, more stringent requirements are needed for the fabrication of metal contacts with very low resistance, good thermal stability, and flat surface morphology. It is widely known that parasitic resistances, in the form of contact resistance, significantly affect the overall performance of the electronic and optical devices. The large voltage drop across the semiconductor/metal interface at the ohmic contacts will seriously lead to the loss of device performance and reliability, for instance, in LEDs the power loss at the contacts will reduce the wall-plug efficiency and increase the junction temperature. This potentially degrades the operating lifetime. Therefore, high quality, thermally stable contacts to GaN-based materials are essential for the fabrication of reliable, efficient, high performance devices and circuits.

A wide variety of metallizations for ohmic contacts on n-GaN have been intensively investigated. From the literature, contact resistances below $10^{-5}$ Ω-cm$^2$ can be achieved routinely and low contact resistance as low as $10^{-8}$ Ω-cm$^2$ has been reported (Lin, *et al* 1994, Fan, *et al* 1996), which is good enough for the optical and electronic devices. However, for p-type GaN, the typical values of contact resistance are higher than $10^{-4}$ Ω-cm$^2$. Low-resistance ohmic contact to p-GaN is difficult to obtain due to the difficulty in achieving high carrier concentration (~$10^{18}$ cm$^{-3}$ and above), and the absence of suitable metals with high work function, larger than band gap and electron affinity of GaN (7.5 eV) (Liu and Lau, 1998, Jang, *et al* 1999). These two obstacles have impeded the fabrication of highly efficient blue LEDs and LDs. Table 2.3 summarizes some of the common contact metallizations used by researchers for p-GaN.

Table 2.3: The overview of some published data on metal contacts/p-GaN

| Metallization | Annealing (ºC) | Duration (min.) | $\rho_c$, ($\Omega cm^2$) | Remark | Reference |
|---|---|---|---|---|---|
| Ni/Au | 300 | 3 | $9.2\times10^{-2}$ | -- | Cao and Pearton, 1998 |
| | 450 | 15 | 0.1 | -- | Wenzel, *et al* 2001 |
| | 400 | 5 | $3.31\times10^{-2}$ | sputtered | Delucca, *et al* 1998 |
| | 400 | 10 | $1\times10^{-4}$ | Using air during heat treatment | Ho, *et al* 1999 |
| | 500 | -- | $2.7\times10^{-3}$ | e-beam evaporator | Hu, *et al* 2006 |
| | 800-900 | -- | $3\times10^{-4}$ | $TiB_2$ as diffusion barrier | Voss, *et al* 2006 |
| Au | 450 | 15 | 1 | Non-ohmic contact | Wenzel, *et al* 2001 |
| | -- | -- | $2.6\times10^{-2}$ | | Mori, *et al* 1996 |
| Ni | 400 | 5 | $3.4\times10^{-2}$ | Thermal evaporation | Delucca, *et al* 1998 |
| Pd | 450 | 7.5 | 0.2 | -- | Wenzel, *et al* 2001 |
| Pt | 475 (5min.) | 35 (accum.) | 1.5 | Non-ohmic contact | Wenzel, *et al* 2001 |
| | -- | -- | $1.3\times10^{-2}$ | | Mori, *et al* 1996 |
| | 600 | 1 | $1.5\times10^{-2}$ | Electro deposited | Delucca, *et al* 1998 |
| Au/Pt | 350 | -- | $4.2\times10^{-4}$ | -- | King, *et al* 1998 |
| Pd/Au | -- | -- | $4.3\times10^{-4}$ | Surface treatment | Kim, *et al* 1998 |
| Pt/Ni/Au | 350 | 1 | $5.1\times10^{-4}$ | -- | Jang, *et al* 1999 |
| Pt/Re/Au | 600 | 1 | $1.4\times10^{-3}$ | -- | Reddy, 2005 |

### 2.4.2 Schottky contact on GaN

The Schottky barrier height to n-GaN for a variety of elemental metals has been studied intensively. The reported barrier height (as shown in Fig. 2.8) increases monotonically but does not scale proportionally with metal work function. The barrier heights ranging from ~1.3 eV for Pt to 0.25 eV for Ti have been observed with considerable amount of variation in the experimental results for a given metal. The strategy to form ohmic contacts on n-GaN would be to use a metal with a small work function such as Ti and Al, on the other hand, to use a metal with large work function

such as Pt to form Schottky barriers on n-GaN. A survey of the literature shows that this principle is generally followed in fabricating contacts on n-GaN.

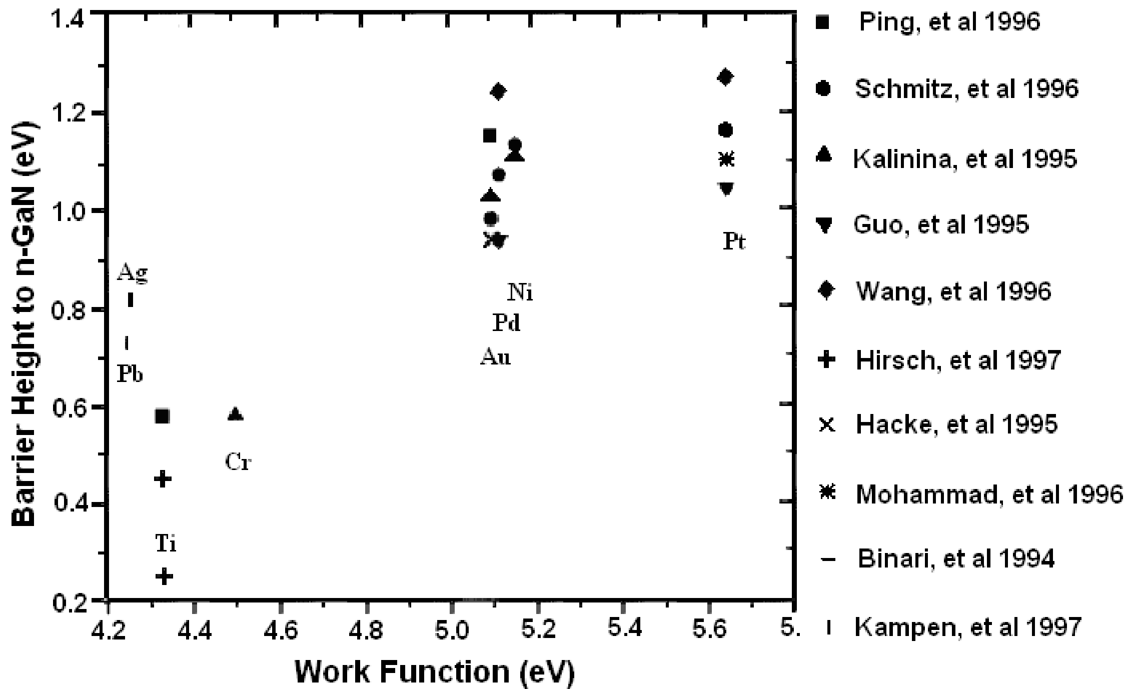


Fig. 2.8. Reported barrier heights of metals to n-GaN as a function of their work function (adapted from Liu and Lau, 1998)

Small measured values of the Richardson constant, A** as compared to theoretical value, and the ideality factor, n which is significantly greater than unity are the commonly observed non-ideal behaviour of GaN Schottky diodes which can be caused by several factors. For instances, surface defects which lead to inhomogeneities in the transport current, or several transport mechanisms operating at the same time or both. GaN grown by various techniques is known to produce high density of structural defects, these defects are likely to be the primary reason for non-ideal I-V curves and small experimental values of A**. Another crucial factor affecting the properties of Schottky contacts on GaN and metal contacts is the metal-semiconductor (MS) reactions. MS reactions are known to depend strongly on the interface. Interfacial reaction between contact metal and semiconductor frequently